(12)

Application of Solidification Theory to Rapid Solidification Processing

W. J. Boettinger, J. W. Cahn, S. R. Coriell,
J. R. Manning, and R. J. Schaefer
Metallurgy Division
Center for Materials Science
National Bureau of Standards
Washington, DC 20234

Semi-Annual Technical Report
Period Covered: October 1, 1981 to March 31, 1982

Report Issued: September 1982

Prepared for
Defense Advanced Research Projects Agency
Arlington, Virginia 22209

Program Code No: 9D10
Effective Date of Contract: April 1, 1979
Contract Expiration Date: March 31, 1984
Principal Investigator: J. R. Manning (301/921-3354)

Table of Contents

Application of Solidification Theory to Rapid Solidification Processing

1. Technical Report Summary

This semi-annual technical report for ARPA Order 3751 covers the period October 1, 1981 to March 31, 1982. Significant accomplishments during that period were achieved in the following areas:

Extended Solid Solubilities -- for Production of Alloys with New Compositions and Phases

- At high growth rates in Ag-Cu alloys, microsegregation-free single phase structures were obtained for all compositions investigated, thus confirming that extended solid solubility could be obtained completely across the phase diagram in this alloy system.
- It was found that the solidification velocity required to produced this single phase structure was lowest for dilute alloys and alloys near the eutectic composition, consistent with theoretical predictions.
- At intermediate growth rates, for Ag-Cu alloys with 9% Cu or greater, structures consisting of alternate bands of segregated and segregation-free material were obtained.

Interface Stability -- for Production of More Homogeneous Alloys

- Influence of trace impurities on interface stability during solidification of dilute Al alloys was analyzed and strong destabilizing effect for some elements was found.
- Structural variation with composition which cannot be explained in terms of conventional cellular patterns was observed in in Al-Mn alloys.

- o Electron beam surface melting procedures were developed which allow the formation of continuous deep rapidly solidified layers.

Interface Kinetics -- for Production of Alloys with Finer Segregation

- o A theory was developed to predict the effect of interface attachment kinetics on the growth rate of dendrites in supercooled metals.
- o A kinetic coefficient equal to 200 cm/(sK) was estimated for pure nickel from the sound speed; this value provides a good fit to dendritic growth data at high velocities.

Prevention of Cracking Caused by Residual Stress -- for Production of Alloys with Improved Surface Structures

- o Response of three different types of metals to the residual stresses developed during electron beam surface melting was characterized.

Task Objective

The objective of this work is to develop guidelines based on kinetic and thermodynamic solidification theory for prediction and control of rapid solidification processes. In particular, segregation effects and rules governing the formation of equilibrium and non-equilibrium phases, including metallic glasses, will be investigated. Areas where significant improvements in alloy properties can be produced by rapid solidification will be emphasized.

Technical Problem and General Methodology

Rapid solidification techniques make it possible to produce new types of materials having significantly better properties than conventionally processed materials. However, improved predictive techniques and control

of rapid solidification processes are needed. The current studies are focussed on the science underlying areas where improved materials can be obtained in order to provide such prediction and control. This work is both theoretical and experimental.

Three major ways in which rapid solidification technology provides improved materials are:

A. Production of alloys with new compositions and phases

B. Production of more homogeneous alloys.

C. Production of alloys with improved microstructures, including finer segregation, and improved surface structures

The general method followed in this work has been to identify critical questions in these three major rapid solidification application areas where solidification theory, when properly developed and checked by experiment, can provide improved understanding of important rapid solidification processes. This understanding then is pursued to provide guidelines that can be used by alloy producers to obtain new improved materials and to select optimum alloy compositions and processing conditions for rapid solidification applications.

Accomplishments to date on this contract and work in progress in each of these areas will now be described in more detail.

Summary of Technical Results, Important Findings, Plans and Implications for Future Work

In application A, particular success has been achieved during the first three years of this contract in (1) evaluating conditions which control critical solidification velocities for production of metallic glass alloys,

and (2) determining conditions that control achievement of extended solid solubilities in rapidly solidified alloys. The work on critical solidification velocities for metallic glass formation is nearing completion. Emphasis now is on investigations of extended solid solubilities. Important findings and planned future work on these metallic glass and extended solid solubility types are discussed, respectively, in the following two paragraphs.

(1) By rapid quenching of Pd-Cu-Si alloys of varying copper composition, NBS investigators were able to determine maximum solidification velocities for dendrite and eutectic crystallization and, consequently, the conditions for glass formation. A sharp transition from crystalline to amorphous solidification was consistently found when the solidification velocity was increased above about 2-20 mm/s in these alloys, depending on composition. These results then were used to relate glass-forming tendencies to phase diagram features as well as to kinetic models of crystallization based on the diffusional sorting of solute in the liquid. At some compositions and velocities, independent nucleation of crystallites occurred even in the presence of a substrate. Nevertheless, the experimental results generally confirmed the importance of solute redistribution on the maximum crystal growth rate in these alloys. Crystal growth rates rather than nucleation rates were the main factor in determining whether amorphous or crystalline solidification was obtained. In carrying out this work, a directional solidification apparatus was built which allowed direct knowledge of fast solidification velocities. These velocities usually have not really been known in previous rapid solidification investigations.
(2) Principles which allow prediction of maximum thermodynamic limits on extended solid solubility in rapidly solidified alloys and phase sequences

for metastable alloys have been formulated. However, because of kinetic limitations, it may in some cases not be possible to obtain the amounts of extended solid solubility that would be thermodynamically allowed. Experiments are being performed to test the predicted kinetic and thermodynamic limits on extended solid solubility. Here again, it will be important to establish the rapid solidification velocities that are sufficient to prevent the sorting of constituents into two-phase rather than one-phase structures. Electron beam surface melting and refreezing of Ag-Cu alloys is being used to investigate these effects more thoroughly.

In application B, it was predicted that, when solidification occurs rapidly enough, the stable shape of the solidification interface is planar rather than cellular or dendritic. Then, interdendritic alloy segregation will be avoided and a more nearly homogeneous alloy obtained. Planar interfaces are also stable at very slow velocities. However, at intermediate velocities, nonplanar (cellular or dendritic) interfaces are produced. Calculations indicate that the high velocity planar regime will occur at practical rapid solidification rates in a number of alloys. Experiments are being performed on aluminum alloys to test this prediction. An electron beam melting system has been modified to produce a measurable energy distribution in the beam during surface melting. When this beam is pulsed or scanned across the surface, solidification velocities produced during the refreezing process can be calculated to allow comparison of experimental observations with theory. Conditions under which stable interfaces can be maintained are being investigated as a function of solidification velocity and alloy composition. While elements having high solute distribution coefficients, k, such as manganese and silver, should not be destabilizing even at rather high concentrations (fractions of one percent)

at solidification velocities of 1 to 10 cm/s, results to date indicate that other solutes, such as nickel, tin, or iron, having much lower distribution coefficients can cause instability at these same velocities when present in much lower concentrations. Investigations of the microstructures formed in these alloys, their causes, possible effects of non-equilibrium at the interface, and implications for rapid solidification processing are continuing.

In application C, three effects of rapid solidification on alloy microstructure are being investigated; (1) microsegregation in rapidly solidified alloys, (2) formation of amorphous layers on alloy surfaces, and (3) stresses leading to cracking of rapidly solidified surfaces are being investigated.

(1) A large number of alloys can be expected to exhibit cellular growth and consequent fine scale intercellular segregation even at very high solidification velocities. To investigate this segregation a quantitative theory of microsegregation during rapid solidification has been formulated which shows the influence of cellular spacing, solidification velocity, and the amplitude of the instability at the interface on the magnitude and distribution of the intercellular segregation. This fine-scale segregation is important because of the precipitation processes that may be produced and because of the well-known correlation between segregate spacing and mechanical properties.

(2) Methods have been devised for producing, on Pd-Cu-Si substrates, by electron beam surface melting and refreezing, continuous amorphous layers up to 200 μm thick without optically visible crystals being formed. The formation of glassy surface layers, particularly if extended to other alloys, could produce special desirable surface properties on otherwise crystalline materials. The overlapping strip method used to produce these deep glassy layers is also being applied to studies of surface layers in crystalline materials.

(3) Several deleterious effects can result from the residual stresses generated during surface melting, such as cracking in the melt zone or substrate and distortion of the substrate. Cracks produced after electron beam surface melting and refreezing at various sweep velocities and power inputs are being investigated to provide possible guidlines for avoidance of this persistent problem which occurs in many instances where rapid solidification is used for surface modification purposes. Materials with less extreme susceptibility to plastic deformation, hot tearing and brittle fracture will be used to define more clearly the variation of defect structure with processing parameters.

2. Report of Technical Progress and Results

Extended Solid Solubility

The goal of this research is to determine experimentally the solidification velocity required to produce microsegregation-free single phase alloys in the Ag-Cu alloy system. For alloys exceeding the equilibrium solubility, such a microstructure indicates extended solubility. The Ag-Cu system has been chosen because the phase diagram has a simple eutectic between two fcc phases and the thermodynamic functions are sufficiently well-known to permit a determination of the T_0 curve, which is the locus of points on the phase diagram where the liquid and solid free energies have the same value. In addition, the metastable solidus curves of the Ag- and Cu-rich phases appear to be retrograde such that solubility extension beyond these retrogrades must be accomplished by solute trapping.

Two solidification mechanisms can produce segregation-free crystalline solids: planar growth and partitionless solidification. The solidification conditions required for planar growth with equilibrium partitioning at the interface are well known. For growth at high velocities, capillarity provides a stabilization of the planar interface. This regime is referred to as absolute stability and applies only when the net heat flow is toward the solid. Partitionless solidification arises from the kinetics of interface motion. Solute is trapped by the moving interface causing the partition coefficient to deviate from the equilibrium value. Solute trapping occurs at high interface velocities when the interface temperature is below a temperature determined from thermodynamic considerations. In the limit of partitionless solidification, when the partition coefficient is unity, this temperature is the T_0 temperature for the composition at the interface. A major goal of this research is to determine the relative contribution of these two mechanisms.

Alloys were prepared for electron-beam surface melting by induction melting of 99.99% pure components in a graphite crucible under vacuum and chill casting in a carbon-coated copper slab mold. Ingots were cold-rolled to 3 mm thick sheets. For the surface melting experiments, the substrate must be prepared with either no microsegregation or microsegregation fine enough to ensure complete mixing during surface melting. The following procedure was found to be adequate for solidification at velocities up to 400 cm/s. Alloys containing 1 and 5 wt% Cu were homogenized for 20 hrs. at 750 °C. Alloys containing 9, 15 and 23 wt% Cu were surface melted using overlapping electron-beam passes to a depth of ~ 0.5 mm at a scan speed of 3 cm/s. This produces a dendrite arm spacing in the range of 1 μm. These slabs were then rolled slightly to eliminate surface topography produced by the e-beam melting. Alloys containing 28.1 wt% Cu (the eutectic composition) required no pretreatment due the fineness of the eutectic structure.

Surface melting experiments were performed by electronically scanning a 25 keV electron beam focussed to approximately 1 mm with a current of 50 mA across the surface of the prepared substrates. Scan velocities between 1.5 cm/s and 400 cm/s were possible. At the slow scan speeds welds were typically 0.6 mm wide and 0.2 mm deep while at 400 cm/s the welds were typically 0.2 mm wide and 0.02 mm deep. Samples for metallography were obtained as sections transverse to the scan direction and occasionally the other two perpendicular sections. TEM samples were obtained by punching half disks, 3 mm in diameter, from 0.1 mm thick transverse slices through the weld zone. Thin foils were obtained by ion milling.

Significant effects arise from the change in weld puddle shape as the scan rate is increased. The local solidification velocity is equal to the product of the scan velocity with the cosine of the angle between the scan direction and the local growth direction. Because of this factor, growth velocities at the top center of the weld puddle for high scan speeds may differ from the scan velocity by a factor of two. Four general types of microstructure are observed depending on solidification velocity and composition. a) At high growth rates, microsegregation-free single phase structures are obtained for all compositions. The velocity required to produce this structure is lowest for dilute alloys and alloys near the eutectic composition. At low growth rates, b) conventional dendritic (cellular) or c) eutectic structures are obtained. d) At intermediate growth rates for alloys with 9 wt% Cu or greater, a structure consisting of alternate bands of segregated and microsegregation-free material is obtained. The bands form parallel to the local interface. The growth rates required to cause the various changes in microstructure for the different compositions will be described in the future.

Experiments on Interface Stability and Segregation with Electron Beam System

Electron beam surface melting can provide a very well-controlled method for producing rapidly solidified regions on the surface of bulk metal substrates. The electron beam facilities at NBS, and the techniques for operating them, have been continuously upgraded so that it has become possible to better characterize the melting conditions and to make deeper, smoother, and more uniform layers of rapidly solidified material for metallurgical evaluation.

One important objective of rapid surface solidification is to produce highly homogeneous surface layers. We report here work relating to achieving this objective by two different methods;

(a) by crystalline solidification at high velocities and

(b) by the formation of continuous layers of metallic glass

Analysis of the influence of several different solutes on the morphological stability of aluminum during rapid solidification has indicated that while elements having high solute distribution coefficients, k, such as manganese and silver, can be present in rather high concentrations (fractions of one percent) without causing interfacial instability at solidification velocities of 1 to 10 cm/s, other solutes such as nickel, tin or iron having much lower distribution coefficients can cause instability at these same velocities when present in much lower concentrations, on the order of 10^{-4} percent. Assuming equilibrium partitioning of solute at the solid-liquid interface, the relative influence of the low k elements is greater at higher velocity (the absolute stability regime). If, however, the solidification velocity is sufficiently high to give non-equilibrium partitioning effects (solute trapping), then the relative influence of low k elements may be greatly diminished. In

the velocity region where the distribution coefficient varies strongly with velocity, the stability analysis becomes much more complex. Unfortunately very little information is available concerning the velocity dependence of k.

As a result of these considerations it is probable that minute amounts of impurities such as iron account for our observation that aluminum containing Mn or Ag is less stable than predicted at solidification velocities of a few centimeters per second but can nonetheless be made stable at high concentrations by solidifying at velocities which may be sufficient to produce solute trapping (as produced by melt spinning).

Metallographic analysis of electron beam melt spots on Al-Mn alloys showed a structural variation with composition which is difficult to explain in terms of a conventional cellular structure and is suggestive of velocity-dependent distribution coefficient effects. Conditions which in a 1% Mn alloy produce a cellular microstructure which is very strongly lamellar in a longitudinal section produced in an 0.1% Mn alloy a structure which in the same longitudinal section appears much more like a three-dimensional network of cells. A complete characterization of this structure, however, will require simultaneous determination of its appearance in orthogonal sections. Comparison with the theory of interface stability including the effects of a velocity-dependent distribution coefficient is rendered difficult by the absence of any information on the form of k(v) and the possible influence of minute concentrations of impurities.

The most extreme case of a homogeneous metallic solid is the metallic glass, and we have found that electron beam surface melting can be used to make relatively thick extensive layers of amorphous materials. This

study used palladium-copper-silicon alloys in which it is known that coupled growth of the crystalline phases cannot take place at velocities of greater than a few millimeters per second. Such sluggish growth kinetics suggested the possibility that if the electron beam is scanned rapidly across the surface to produce a single amorphous melt pass, which is known to be quite easy in this material, then successive overlapping passes could be used to generate additional amorphous material without resulting in significant crystallization in the previous passes. Thus even though the amorphous material is raised to a high temperature by successive passages of the electron beam, any crystals which might form cannot grow more than a few microns before the local region again cools to ambient temperature.

The strategy used to produce continuous amorphous layers was thus to start with a crystalline slab 6-8 mm thick, form a line of amorphous material by a single sweep of the electron beam across the surface, allow sufficient time for the sample to cool thoroughly, and then sweep the electron beam across the surface again, offset from but overlapping the first sweep. The process was continued to generate a strip of any desired width of overlapping melt passes. The time allowed between successive passes was 30 or 60 seconds. This time was more than enough to allow the amorphous material to cool to a temperature close to that of the substrate, but was kept long to allow sufficient transfer of heat from the substrate to the water-cooled copper chill plate below it. The individual melt passes were approximately 1 mm wide and the offset between passes was typically 0.5 mm.

Continuous amorphous strips were formed by this process, although usually with extensive cracking of the substrate as discussed in another part of this report. Crystals which were present within the melt zones

had microstructures indicative of growth radially outward from nucleation sites, thus indicating that the sweep speed of the electron beam is significant not because of any possibility of the crystals growing with this speed but because it determines the time which the local region may spend at elevated temperature.

Crystallization of previously formed metallic glass by subsequent melt passes was concentrated near the bottom of the melts with the result that a continuous layer of glass remained near the surface if the sweep speed was sufficiently high. Material transport by the moving beam was extremely prominent in these experiments, with the result that the final surface was greatly depressed below the original surface in the region where the melt passes started, and elevated above the original surface by a corresponding amount at the opposite end.

Using the overlapping scan method, continuous glassy layers up to 200 μm thick without optically visible crystals were formed. This required sweeping the electron beam across the surface at velocities of 60 cm/sec or more. Further optimization of processing parameters could result in thicker amorphous layers, since the overlap method has been shown to work and some glass was formed at depths of over 500 μm.

When the same process is attempted with Cu-Zr, very little glass is formed. Although this is also a relatively easy glass former, when the melts are several hundred micrometers deep the cooling rates are not sufficient to prevent the crystals in the substrate from growing up to the surface in most places.

In addition, attempts to produce a wide strip of thick glassy material on Pd-Cu-Si by rapidly (several kHz) oscillating the electron beam in the direction perpendicular to that with which it swept over the surface of

the slab resulted in amorphous material only along the sides of the strip. Although no heat flow analysis of this melting mode has been carried out, it is clear that the attainable cooling rates are slow except at the edges of the strip or for very thin melts. The overlapping strip method as described above is thus the most effective way to obtain deep layers of rapidly solidified material, and it is being applied to studies of surface layers in crystalline materials, where the transient heating of the earlier melts is not as critical as in the glassy materials.

Theory of Interface Kinetic Effects and Interface Stability

Significant departures from local equilibrium at the crystal-melt interface can exist for solidification at rapid rates. Perhaps, the highest measured crystal growth velocities (50 m/s) are those of Ni dendrites growing into pure undercooled melts as reported by Walker and Colligan and Bayles. Recent theoretical (Langer and Muller-Krumbhaar) and experimental (Glicksman et al.) advances in our understanding of dendritic growth allow accurate calculation of the heat transport limited rate of dendritic growth as a function of melt undercooling. Inclusion of interface kinetics into the heat transport model of dendritic growth has been performed in collaboration with Professor David Turnbull to extend the model to high solidification velocities. We have used previous results on the effect of interface kinetics on the morphological stability of a solidifying sphere to calculate the effect of interface kinetics on the dendritic tip radius and hence the growth rates. An interface kinetic coefficient based on the estimated velocity of sound in molten nickel provides a good fit to the dendritic growth data at high velocities as a function of melt undercooling.

The details of this research are given in an appendix in a manuscript, "Relative Roles of Heat Transport and Interface Rearrangement Rates in the Rapid Growth of Crystals in Undercooled Melts," by S. R. Coriell and D. Turnbull to be published in Acta Metallurgica.

Prevention of Cracking Produced by Electron Beam Surface Melting and Refreezing

Surface layers of rapidly solidified material can be produced on bulk metal substrates by pulsed or scanned energy beams (lasers or electron beams). Such layers may have improved hardness, wear or corrosion resistance, or other desirable properties but in many cases the potential benefits are offset by the harmful effects of the residual stresses developed during the surface melting process. The origin and the effects of these stresses are essentially the same as those developed during conventional welding processes, but the magnitude of some of the controlling parameters such as temperature gradients may be significantly different.

Several deleterious effects can result from the residual stresses generated during surface melting. The most important can be listed as follows:

(a) The most severe type of defect arising from surface melting is cracking, which may occur in the melt zone or the substrate or both. The prevalence of this type of defect is dramatized by the frequent publication of photomicrographs of surface melts containing conspicuous cracks, when the authors would presumably prefer to have obtained melts without cracks.

(b) The residual stresses from surface melting can also cause severe distortion of the substrate. This problem becomes dramatically clear when one attempts to carry out surface melting of large areas on relatively thin (less than about 5 mm thick) substrates.

(c) The inhomogeneous nature of the residual stresses can be expected to provide a multitude of favorable sites for stress corrosion cracking and other forms of electrochemical degradation.

(d) The fact that surface melting almost always results in a surface which is in a state of tensile stress means that even if cracks are not present immediately after solidification, the surface will still be a favorable site for crack initiation.

The importance of these different effects will depend upon the alloy being melted, the application for which it is intended, and the mode of surface melting which is employed. Because little attention has until now been devoted to these effects, we have started studies of residual stress effects with the ultimate objective of identifying procedures which may ameliorate or eliminate the problems.

The most practical way to produce extensive rapidly solidified surface layers on a metal is to scan an energy beam over the surface of a material to produce a continuum of overlapping small weld lines. This mode of melting can be contrasted to the mode frequently used for laser annealing of semiconductors, in which a pulsed laser beam melts a wide but extremely shallow layer on the material surface. In the latter case, the heat flow is one-dimensional and residual stresses may be small or absent but this mode of melting is impractical for most metallurgical applications where deeper melts are desired.

When a small melt spot is scanned across the surface of a metal, the deleterious effects mentioned above have their origin in the thermal contraction of the solid material as it cools, and in some cases also in the change of volume which accompanies solidification. As the scanning velocity of the melt spot increases, the heated area surrounding the melt zone changes in shape and size and the response of the system to the stresses developed during cooling also changes. Realistic analysis of the stresses developed during this type of process is rendered difficult by the temperature dependent elastic/plastic behavior and, especially in the case of highly alloyed materials, the possibility of large deviations from equilibrium during solidification. Of particular importance in surface melting of many alloys are hot tearing phenomena in which cracks form by the pulling apart of the material in the solute-rich regions between dendrites or between grains.

For the case of melting by a circular energy spot scanned across a metal surface, it has been shown (1) that the critical parameters controlling the melting are qa and $Ua/2\alpha$, where q is the absorbed power density, a is the spot radius, U is the velocity with which the spot moves, and α is the thermal diffusivity. For a stationary spot on a given material, a critical value of qa is needed to initiate surface melting and the surface reaches the vaporization temperature at a higher critical value of qa (2). The latter condition bears a relation to the development of the deep penetration mode of welding, which is not generally desired for surface melting. As a result the range of useful values of qa for surface melting is relatively narrow, from approximately 2.3×10^5 W/m to 4×10^5 W/m for aluminum. When the energy spot moves, the melt pool does not differ

greatly in shape from the stationary spot for $Ua/2\alpha$ values less than unity. Although the shape of the melt pool has not been computed for $Ua/2\alpha>1$, it is clear that the melt pool trails increasingly far behind the moving spot and that the rear edge becomes increasingly pointed. With increased velocity the melt pool also diminishes in size and eventually disappears unless the $q\alpha$ value is simultaneously increased. These changes in shape of the melt pool with increasing velocity lead to changes in the residual stress patterns.

Electron beam surface melting by this type of scanned circular spot produces different residual stress reactions in different alloys, as is expected on the basis of elastic/plastic properties and solidification phenomena. In some cases the residual stress effects vary significantly with the melt scan velocity. In our experiments, melts were carried out by electronic deflection of a 25kV electron beam at velocities from 2 to 100 cm/sec. The free surface and/or polished sections were examined for evidence of residual stress related defects.

In pure aluminum cracks cannot be generated by either hot tearing during solidification or subsequent brittle fracture. Instead, this material responds to the generated stresses by plastic deformation, and if the surface is sufficiently clean an abundance of slip lines become visible. Those slip lines extend across the surface of the melt zone and extend without discontinuity into the matrix on either side. At high velocities the slip lines are more prominent and are visible at a larger distance to the side of the melt path than they are at lower velocities. It is not clear, however, if this difference indicates a greater amount of slip at high velocities, or a concentration of the slip

into a smaller number of more visible bands. Further experiments using single crystal substrates may resolve this question.

When repeated overlapping melts are carried out on pure aluminum to produce a rapidly solidified surface layer, the free surface is covered with a pattern of intersecting slip lines which strongly resemble the scratches on a partially polished metallographic sample. In some cases these slip lines could be the limiting factor with respect to the smoothness of the treated sample surface, but usually they are rather small in amplitude compared to the overall surface relief caused by the melting process.

In contrast to pure aluminum, 2024 alloy with its high copper content shows extensive cracking in response to surface melting. A series of melts was made on this alloy using q_0 values between 3×10^5 and 5×10^5 w/m at velocities from 2.5×10^{-2} to 1 m/s, corresponding to $U_0/2a$ from 0.05 to 2. In these experiments the electron beam radius a was held constant at approximately 3.5×10^{-4} m. Within this range of parameters, the cracking pattern showed little evidence of variation with q_0 but a clear variation with velocity. Slip lines were never seen in this material.

All of the cracks which were observed appeared to be hot tearing - i.e., they occurred in solute-rich regions, either between grains or between dendrites.

At velocities of 5×10^{-2} m/s or less, cracks were very small and were frequently interdendritic as well as intergranular. They showed a strong tendency to lie perpendicular to the local solid-liquid interface, the shape of which is delineated by surface ripples.

At a sweep velocity of 10^{-1} m/s, severe cracking becomes evident. This occurs mostly in the form of a single large crack running along the center line of the melt pass. Occasional cracks are also present running inward from the sides of the melt, but they are smaller than the central crack and are usually not directly connected to it. At this velocity and at all higher velocities, the cracks occur almost exclusively along grain boundaries.

As the velocity with which the electron beam sweeps over the surface is increased up to 1 m/s, the cracks running in from the sides of the melt become more prominent and the crack along the center line of the melt pass becomes relatively smaller and more discontinuous. At the highest speeds, the tendency of the cracks to run perpendicular to the local solid-liquid interface, as delineated by the surface ripples, decreases.

In the velocity range close to 10^{-1} m/s, where cracking occurs primarily along the center line of the melt, an extended area of relatively crack-free surface melt can be produced by overlapping subsequent melt passes far enough to remelt the center line cracks.

A totally different type of cracking was seen in the glass-forming palladium-copper-silicon alloys when overlapping melt tracks were used to produce a continuous glassy surface layer. The glassy layer is ductile, and all cracking occurred in the substrate. Frequently the fracture took the form of a very large single crack, lying under the glassy layer and at a depth up to two or three times the depth of the melt zone. This crack would often emerge at the free surface of the metal on either side of the surface melted strip. Some cracks from the substrate were also

seem to impinge upon the surface melted layer and to be stopped by the amorphous material, often with considerable plastic deformation of the latter. From these crack patterns, and from the occasional direct observation of actual crack formation, it is clear that most of these cracks form at some time several minutes after the completion of the surface melting process.

In conclusion, the different behavior of the three materials discussed here can be understood in terms of their relative susceptability to plastic deformation, hot tearing and brittle fracture. These three materials, however, represent rather extreme cases of susceptability to these processes. For example, the silver-copper alloys discussed in a different part of this report do not show any hot tearing even in highly alloyed samples. Future studies will therefore use materials with less extreme susceptability to these processes, to more clearly define the variation of the defect structure with processing parameters.

References

1. S. Kou, S. C. Hsu, and R. Mehrabian, Met. Trans. 12B, 33-45 (1981).

2. S. C. Hsu, S. Kou, and R. Mehrabian, Met. Trans. 11B, 29-38 (1980).

APPENDIX - Paper to be published in Acta Metallurgica

Relative Roles of Heat Transport and Interface Rearrangement Rates in the Rapid Growth of Crystals in Undercooled Melts

S. R. Coriell and D. Turnbull*
National Bureau of Standards
Washington, DC 20234

Abstract

Perhaps, the highest measured crystal growth velocities (50 m/s) are those of Bi dendrites growing into pure undercooled melts as reported by Walker and Colligan and Bayles. Recent theoretical (Langer and Muller-Krumbhaar) and experimental (Glicksman et al.) advances in our understanding of dendritic growth allow accurate calculation of the heat transport limited rate of dendritic growth. We use previous results on the effect of interface kinetics on the morphological stability of a sphere to calculate the effect of interface kinetics on dendritic growth. An interface kinetic coefficient based on the estimated velocity of sound in molten nickel provides a good fit to the dendritic growth data at high velocities.

---

* Permanent Address: Division of Applied Sciences, Harvard University, Cambridge, MA 02138

The constraints imposed by capillarity on the disposal of the heat released in crystal growth have been evaluated in several recent publications (1-8). These evaluations have increased the accuracy with which the upper limiting rates of crystal growth (i.e., the heat transport limited rates) can be computed. The rates of growth of crystals into undercooled metal melts are thought to approach these upper limiting rates closely, reflecting relatively high rates of the melt → crystal interfacial rearrangement processes. In this near heat transport limited regime the displacement, ΔT_i, of the crystal-melt interface temperature, T_i, from the thermodynamic equilibrium temperature, T_m, is negligible compared with $\Delta T = T_m - T$, where T is the ambient, i.e., heat sink, temperature. However, if the interface moves ΔT_i must be displaced from zero by an amount proportional, near equilibrium ($T_m >> \Delta T_i$) and with the fraction (f) of interfacial growth sites constant, to the rate, V, of the observed motion. In particular, (9)

$$V = V_o \frac{\Delta S_f}{\bar{N} k_B} \frac{\Delta T_i}{T_i} \qquad (1)$$

where ΔS_f is the molar entropy of fusion at T_i, $\bar{N}$ is Avogadro's number, and k_B is the Boltzmann constant. V_o is a kinetic constant proportional to the interfacial rearrangement frequency and f. It can hardly exceed the limit, which should be of the order of the sound speed v_s, imposed by the collision frequency of atoms or molecules from the liquid onto the interface (9, 10). Thus

$$V \leq v_s \frac{\Delta S_f}{\bar{N} k_B} \frac{\Delta T_i}{T_i} \qquad (2)$$

Exposure of the actual ΔT_i and V_o should be most favored under conditions where the ambient undercoolings and attendant crystal growth speeds are very large.

Perhaps the highest measured crystal growth velocities are those of Ni and Co into their pure undercooled melts, reported by Walker (11) and Colligan and Bayles (12). In their experiments columns of the bulk melt were undercooled by varying amounts up to 250-300° and then seeded at one end. V was determined from the times at which the freely moving dendrite tip passed thermal sensors sited along the column.

The growth rates at given ambient undercooling, ΔT, were fairly reproducible to $\Delta T \gtrsim 0.1T_m$, but scattered widely at $\Delta T > 0.1T_m$, presumably because of the perturbing influence of dynamic nucleation events which frequently accompanied the rapid growth in this ΔT regime. The ΔT dependence of V was approximately described by:

$$V \gtrsim A(\Delta T)^2 \qquad (3)$$

with A = 0.142 and 0.17 cm/(sec $(K)^2$) for Ni and Co, respectively. While still on its parabolic course V in both metals had reached levels near 50 meters/sec at $\Delta T \gtrsim 0.1T_m$. This velocity would require an interfacial undercooling $\Delta T_i \gtrsim 0.015T_m$ since v_s in these liquids is expected to be $\sim$ 3000 meters/sec. Therefore it should be substantially and measurably less than the calculated heat transport limited (i.e., $\Delta T_i = 0$) rate.

This paper presents the theory of heat transport limited crystal growth as modified to allow for the restraints imposed by the interface rearrangement process and its application to the assessment of the relative importance of heat transport and interface kinetics in the growth of Ni crystals in their pure undercooled melts.

For an isothermal dendrite (paraboloid of revolution) with tip radius R propagating at constant velocity V, solution of the heat flow equation leads to the relationship

$$[k_L/(\kappa_L L_v)](\Delta T - \Delta T_i) = p \exp(p) E_1(p), \qquad (4)$$

where $p = VR/2\kappa_L$ is the Peclet number, E_1 is the exponential integral, κ_L is the thermal diffusivity of the liquid, L_v is the latent heat per unit volume and k_L is the liquid thermal conductivity. Equation (4) provides one relationship between the three variables ΔT, V, and R. The theoretical work of Langer and Muller-Krumbhaar (1-2) establishes that a second relationship can be obtained from morphological stability theory. Further, an excellent approximation to the more rigorous result of Langer and Muller-Krumbhaar can be obtained from considerations of the morphological stability of a growing sphere. Such an approximate theory has been shown to provide an excellent fit to the extensive dendritic growth data on succinonitrile (5-6). We will use previous results on the effect of interface kinetics on the morphological stability of a sphere to obtain a second relationship between ΔT, V, and R. By combining this second relationship with eq. (4), we obtain the dendrite growth velocity V as a function of bath undercooling ΔT.

We consider growth into a undercooled liquid of a perturbed sphere of radius R_s. Above a certain radius, perturbations of the form of spherical harmonics $Y_{\ell m}$ grow more rapidly than the sphere. From eq. (13) of reference 13, this radius (above which the sphere is unstable) is given by

$$R_s = \{R^*/2\}\{1 + (M/N)(L + \alpha_1)\} \times \{1 + [1 + 4\,(M/N)(L - 1)\alpha_1/(1 + (M/N)(L + \alpha_1))^2]^{1/2}\}, \qquad (5)$$

with

$$R^* = 2T_M\Gamma/(\Delta T_s) \tag{6}$$

and

$$V_s = (k_L/L_v)(\Delta T_s/R_s)/\{1 + [k_L/(L_v\mu_1 R_s)]\}. \tag{7}$$

In these equations $M = 1 + (1 + k_s/k_L)\ell$, $N = \ell-2$, $L = \frac{1}{2}(\ell-1)(\ell+2)$, $\alpha_1 = k_L/(L_v\mu_1 R^*)$, $\Gamma = \gamma/L_v$, γ is the solid-liquid surface free energy, k_s is the solid thermal conductivity and $\mu_1 = (V/\Delta T_i)$ is the linear interface kinetic coefficient. We have used the subscript s on V, R, and ΔT to indicate that these quantities pertain to the spherical geometry. Eqs. (5-7) are based on the use of Laplace's equation for the thermal field which, strictly speaking, restricts their validity to small values of $k_L(\Delta T - \Delta T_i)/[\kappa_L L_v]$; however the time dependent stability analysis of Wey et al. (14) indicates a larger range of validity of the time independent analysis. Since the radius of the dendrite or sphere is more than an order of magnitude greater than the nucleation radius R*, we have neglected any dependence of the bath undercooling on surface tension.

Eq. (5) gives the radius above which the perturbations grow more rapidly than the sphere itself (see discussion of absolute and relative stability in reference 13); using this value for the radius seems more reasonable than using that above which the perturbation growth rate is positive.

In using the results of morphological stability theory for a sphere to obtain a relationship between ΔT, V, and R relevant to dendritic growth, it is necessary to decide the manner in which the sphere (ΔT_s, V_s and R_s) models dendritic growth. The basic hypothesis is that the dendrite radius is that for which the sphere is at the stability-instability demarcation and we take $R = R_s$. Since V is an interface quantity while ΔT depends in part on the behavior

far from the interface, it is perhaps more reasonable to require that $V_s = V$ rather than $\Delta T_s = \Delta T$. We will actually consider both of these possibilities. We denote as the RV method the case where $R = R_s$ and $V = V_s$ and as the RT method the case where $R = R_s$ and $\Delta T = \Delta T_s$.

The only adjustable parameter is the integer ℓ which is related to the form of the perturbation of the sphere. Since $\ell = 1$ and $\ell = 2$ perturbations grow more slowly than the sphere, we require $\ell \geq 3$. Presumably, ℓ should reflect the symmetry of the crystal, which for a cubic material suggests $\ell = 4$ or 6 although Langer (2-3) has argued for $\ell = 5$ for a cubic material. For $\ell = 4$ and $k_L = k_s$, eq. (5) reduces to

$$R_s = \{R^*/4\}\{83 + 9\alpha_1\}\{1 + [1 + 576\alpha_1/(83 + 9\alpha_1)^2]^{1/2}\}$$

When interface kinetics are sufficiently rapid, i.e., $\alpha_1 \to 0$, R_s is proportional to R^* with the proportionality constant dependent on ℓ and k_s/k_L. For example for $\alpha_1 = 0$, the above equation gives $R_s = 83R^*/2$. We also note that when interface kinetics are included the dendrite can not be isothermal and eq. (4) which is based on an isothermal paraboloid of revolution is a reasonable but not exact approximation. Approximate corrections to eq. (4) have been derived (8).

In the RV method $R = R_s$ and $V = V_s$, and we use eq. (7) to eliminate ΔT_s from eq. (5) and write the right hand side of eq. (5) as a function of R and V. For a finite rate of the interface process eq. (5) gives a transcendental relationship between R and V which is solved numerically. Eq. (4) with $\Delta T_i = V/\mu_1$ is then solved numerically to obtain V as a function of ΔT. For infinite interface kinetics (i.e., $v_s = \infty$), eq. (5) can be solved explicitly, viz.,

$$R^2 = [2T_M\Gamma k_L/(L_V V)][1 + ML/N].$$

In the RT method $R = R_s$ and $\Delta T = \Delta T_s$, and for a given ΔT, R can be calculated from eq. (5); eq. (4) is then solved numerically to find V as a function of ΔT.

Calculations have been carried out for the growth of nickel dendrites. The following values of the physical properties were used:

$k_L = k_s = 0.9$ J/(cm s K)

$\kappa_L = 0.155$ cm^2/s

$L_V = 2350$ J/cm^3

$\gamma = 0.4\ (10^{-4})$ J/cm^2

$T_M\Gamma = 2.9\ (10^{-5})$ K cm

$v_s = 3.0\ (10^5)$ cm/s

$\mu_1 = (V_s \Delta S_f/\bar{N}k_B T_M) = 2.0\ (10^2)$ cm/sK

The values of L_V, T_m and the heat capacity of the melt were taken from the tabulation of Hultgren et al. (15) while the density of Ni at T_m was set equal to 7.9 gm/cm^3 (16). We found no report of the thermal conductivity of molten Ni but the listed k_s of crystalline Ni was obtained by extrapolating the results in the tables of Touloukian et al. (17) to T_m. Since these authors presented arguments that the change in the thermal conductivity of Fe upon melting is quite small we have assumed that $k_L = k_s$ for Ni. The reduced, or scaled, crystal melt interfacial tension, α, is defined by

$$\alpha = \left(\frac{\bar{N}}{V}\right)^{1/3} \frac{\gamma}{L_V}$$

where $\bar{V}$ is the molar volume. Studies of the kinetics of crystal nucleation in undercooled melts suggest (9) that for most metals $\alpha \gtrsim 0.6$ at the onset temperature of measurable nucleation while the theory of Spaepen (18) gives an upper limiting value $\alpha = 0.86$ at T_m for metals crystallizing to a f.c.c. structure. For our calculations we have set $\gamma = 0.4 \times 10^{-4}$ J/cm^2 corresponding to the assignment $\alpha \cong 0.7$ to Ni. The speed of sound in molten Ni could be computed from [see Kleppa (19)] the relation

$$v_s = (B_a/\rho)^{\frac{1}{2}}$$

where B_a is the adiabatic bulk modulus and ρ is the density of the melt. We know of no measurement of B_a of molten Ni. Bundy and Strong (20) report that the isothermal bulk modulus, B_T, of crystalline Ni at T_m is approximately 1.1×10^{12} dynes/cm^2 and that Ni expands about 6% on melting. Invoking the Gruneisen relation between B and volume ($\frac{\partial \ell n B}{\partial \ell n V} \sim -\gamma_G$) with $\gamma_G \sim 2$ we estimate $B_T \sim 0.85 \times 10^{12}$ dynes/cm^2 for molten Ni at T_M. It is likely that B_a exceeds B_T by 10 to 15%; thus our assignment $v_s \sim 3 \times 10^5$ cm/s seems reasonable.

The results of the calculations are indicated by the solid curves in Figures 1-3 for bath undercoolings of 10-200 K. We have indicated the experimental data by the dashed line corresponding to Walker's measurements (11), viz., $V = 0.142\ (\Delta T)^2$ in the undercooling range 20-175 K. While data is available up to 250 K, the scatter becomes very large above 175 K (11). Colligan and Bayles (12) fit their data with $V = 0.28\ (\Delta T)^{1.8}$ which yields higher velocities for $\Delta T < 30$K and smaller velocities for $\Delta T > 30$K than the quadratic expression. The maximum discrepancy is a factor of 1.4 at $\Delta T = 175$ K which gives an indication of the scatter in the measurements. The calculated curves in Figs. 1 and 3 are based on the RV method while Fig. 2 is based on the RT

method. Figures 1 and 2 give results for three different kinetic coefficients, viz., $\mu_1 = \infty$, 200, and 40 cm/(sK). The intermediate value of 200 cm/(sK) was estimated from the speed of sound while the other two values were used to indicate the sensitivity of the curves to the interface kinetic coefficient. In Figs. 1 and 2, $\ell = 4$ was used; Fig. 3 shows how the value of ℓ affects the calculated results. The difference between $\ell = 4$, 5, and 6 is clearly smaller than the discrepancy between theory and experiment and the scatter in the experimental data. For $\mu_1 = 200$ cm/(sK), good agreement between calculated and experimental values are obtained for large values of ΔT. The largest disagreement occurs at small values of ΔT, e.g., at $\Delta T = 20K$, the experimental velocity (calculated from $V = 0.142\Delta T^2$) is 57 cm/s while the RV method (Fig. 1) gives 16 cm/s and the RT method gives 30 cm/s. While convective effects, which have been ignored in calculations, could cause enhanced growth rates, an estimate of the type developed by Glicksman and Huang (21) indicates that such enhancement would be insignificant for the range of supercoolings considered. Better agreement between theory and experiment could be obtained by using different values of the physical properties. For example, if the thermal conductivities and diffusivities are doubled or the surface tension is halved, the velocities at $\Delta T = 20$ and 200 K increase by 90 and 20%, respectively.

It is of interest to examine the magnitude of various quantities at the higher undercoolings. For example, for the RV method with $\ell = 4$ and $\Delta T = 175$ K, the calculated velocity is $5.14(10^3)$ cm/s and the tip radius is $1.83\ (10^{-5})$ cm. Hence, the kinetic undercooling $\Delta T_i = 25.7$ K, the dimensionless quantity, $k_L(\Delta T - \Delta T_i)/[\kappa_L L_v] = 0.37$, and the Peclet number equals 0.30. The Gibbs-Thomson lowering of the melting point $2T_M\Gamma/R = 3.2$ K, which is negligible compared to the total undercooling of 175 K. For the RT method with $\ell = 4$ and $\Delta T = 175$ K, the calculated velocity is $4.28(10^3)$ cm/s and the tip radius is $2.34(10^{-5})$ cm.

Our calculations show that at the largest undercoolings the growth of Ni dendrites into their melt is significantly retarded by the resistance of the interfacial rearrangement process. For example, at an ambient undercooling $\sim 0.1\ T_m$ we calculate that the interfacial undercooling is $\sim 0.015\ T_m$ or 15% of the ambient. At this large undercooling the measured speed of the dendrite tip is, within the experimental and calculational uncertainty, equal to that calculated by assuming that the rate of the interface process is limited only by the collision frequency of melt atoms with the interface. There is no evidence for thermal activation of this process.

Acknowledgments

The authors are grateful for partial support (for S.R.C.) to the Defense Advanced Research Projects Agency. Gratitude is alo expressed to W. J. Boettinger, R. F. Boisvert, M. E. Glicksman, R. J. Schaefer, and R. F. Sekerka for helpful discussions.

References

1. H. Muller-Krumbhaar and J. S. Langer, Acta Met. 29, 145 (1981).
2. J. S. Langer, Rev. Mod. Phys. 52, 1 (1980).
3. J. S. Langer, PhysicoChemical Hydrodynamics 1, 41 (1980).
4. J. S. Langer, R. F. Sekerka, and T. Fujioka, J. Cryst. Growth 44, 414 (1978).
5. S. -C. Huang and M. E. Glicksman, Acta Met. 29, 701 (1981).
6. M. E. Glicksman, R. J. Schaefer, and J. D. Ayers, Metall. Trans 7A, 1747 (1976).
7. R. D. Doherty, B. Cantor, and S. J. M. Fairs, Met. Trans. 9A, 621 (1978).
8. R. Trivedi, H. Franke , and R. Lacmann, J. Cryst. Growth 47, 389 (1979).
9. F. Spaepen and D. Turnbull in: Rapidly Quenched Metals, Eds. N. J. Grant and B. C. Giessen (M.I.T. Press, Cambridge, MA, 1976) p. 205.
10. D. Turnbull and B. G. Bagley, Treatise on Solid State Chemistry (ed. N. B. Hannay) 5, pp. 513-554, Plenum (1975).
11. J. L. Walker, unpublished work presented in Principles of Solidification, B. Chalmers, Chapter 4, John Wiley, 1964.
12. G. A. Colligan and B. J. Bayles, Acta Met. 10, 895 (1962).
13. S. R. Coriell and R. L. Parker in: Crystal Growth, Ed. H. S. Peiser (Pergamon, Oxford, 1967) p. 703.
14. J. S. Wey, A. K. Gautesen, and J. Estrin, J. Crystal Growth 19, 169 (1973).
15. "Selected Values of the Thermodynamic Properties of the Elements," R. Hultgren, R. D. Desai, D. T. Hawkins, M. Gleiser, K. K. Kelley and D. D. Wagman, Am. Soc. Metals, Metals Park, Ohio (1973).
16. Handbook of Chemistry and Physics, (Ed. R. C. Weast) Chemical Rubber Co., Cleveland Ohio.
17. "Thermophysical Properties of Matter," (Eds. Y. S. Touloukian, R. W. Powell, C. Y. Ho and P. G. Klemens) Vol. 1, p. 237, Plenum Press (1970).
18a. F. Spaepen, Acta Met. 23, 615 (1975);
b. F. Spaepen and R. B. Meyer, Scripta Met. 10, 257 (1976).
19. O. J. Kleppa, J. Chem. Phys. 18, 1331 (1950).
20. F. P. Bundy and H. M. Strong, Solid State Physics (Eds. F. Seitz and D. Turnbull) 13, 134, Academic Press, NY (1962).
21. M. E. Glicksman and S. C. Huang, Adv. Space Res. 1, 25 (1981).

Figure Captions

Fig. 1. Dendritic growth velocity of nickel as a function of bath undercooling. Solid curves are calculated for $\ell = 4$ for three values of the interface kinetic coefficient. Experimental growth velocities are indicated by dashed line for which $V = 0.142\ (\Delta T)^2$.

Fig. 2. Dendritic growth velocity of nickel as a function of bath undercooling with the same parameters as Fig. 1. The assumptions of the RV method and of the RT method are used in the calculations of Fig. 1 and this figure, respectively.

Fig. 3. Dendritic growth velocity of nickel as a function of bath undercooling. Solid curves are calculated for $\ell = 4$, 5, and 6 for the estimated kinetic coefficient of 200 cm/(sK). The dashed line indicates experimental data.

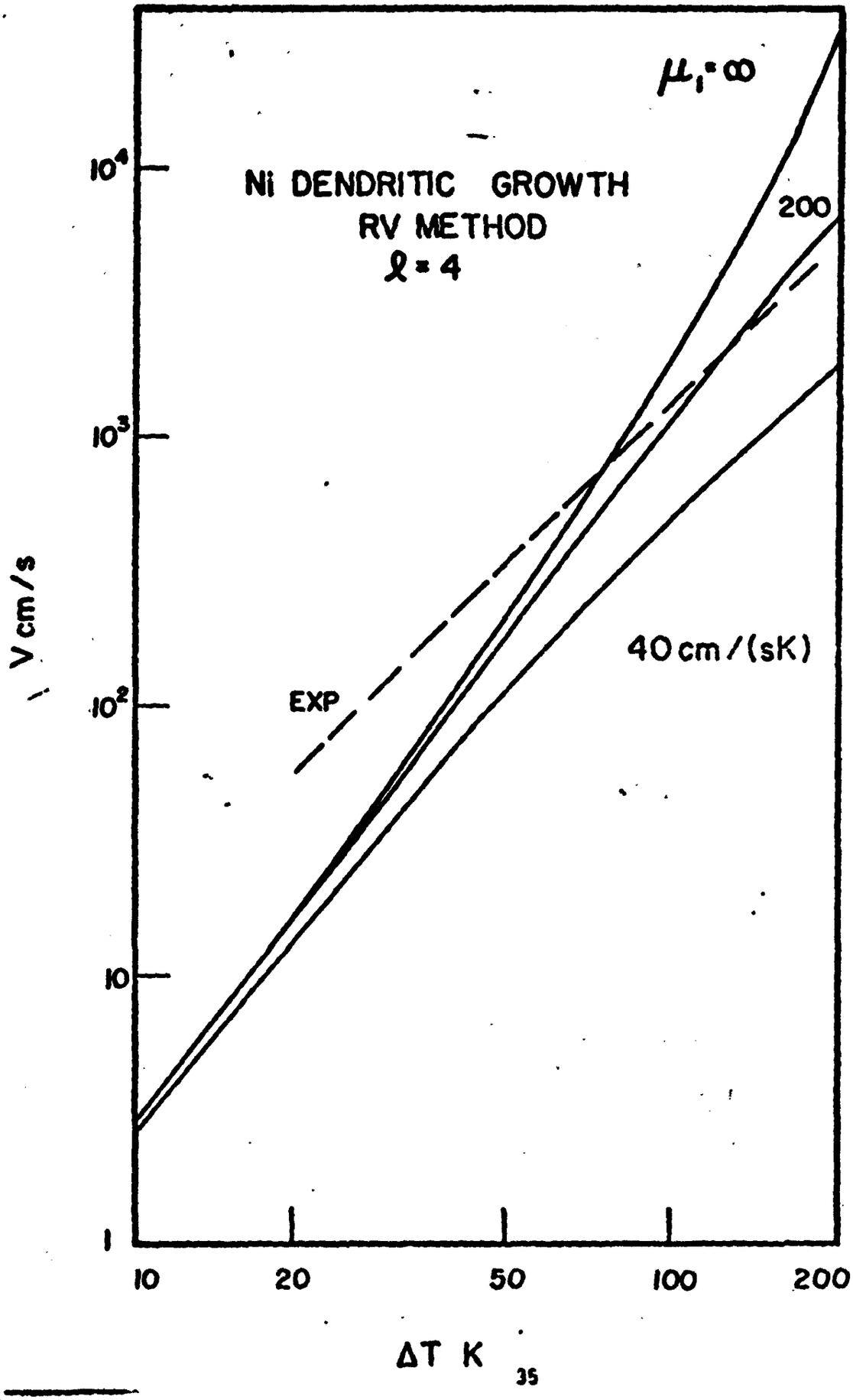
$\mu_i = \infty$
Ni DENDRITIC GROWTH
RV METHOD
$\ell = 4$
200
40 cm/(sK)
EXP
10^4
10^3
10^2
10
1
V cm/s
10
20
50
100
200
ΔT K

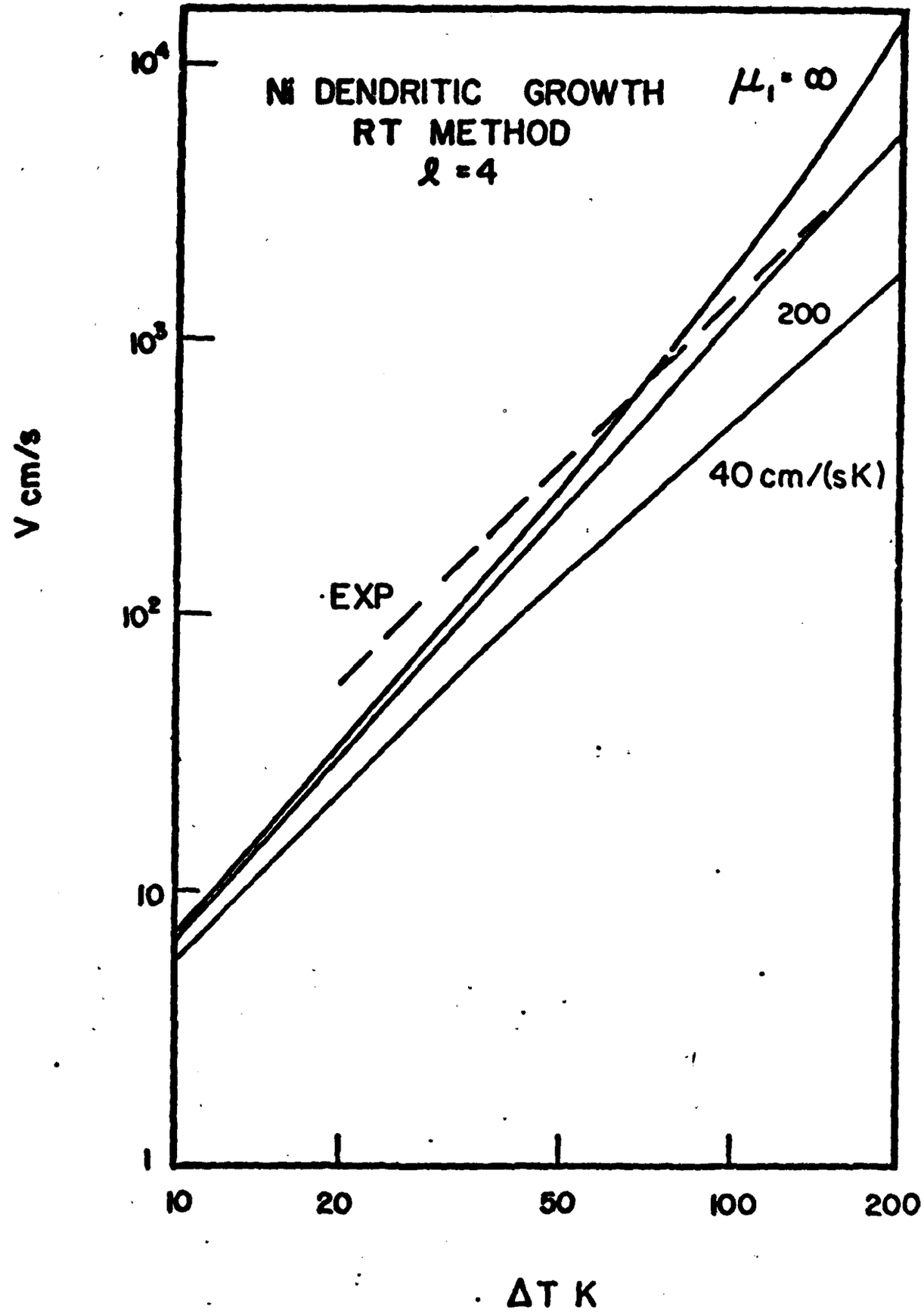
Ni DENDRITIC GROWTH
RT METHOD
ℓ = 4
$\mu_i = \infty$
200
40 cm/(sK)
EXP
V cm/s
10^4
10^3
10^2
10
1
10
20
50
100
200
ΔT K

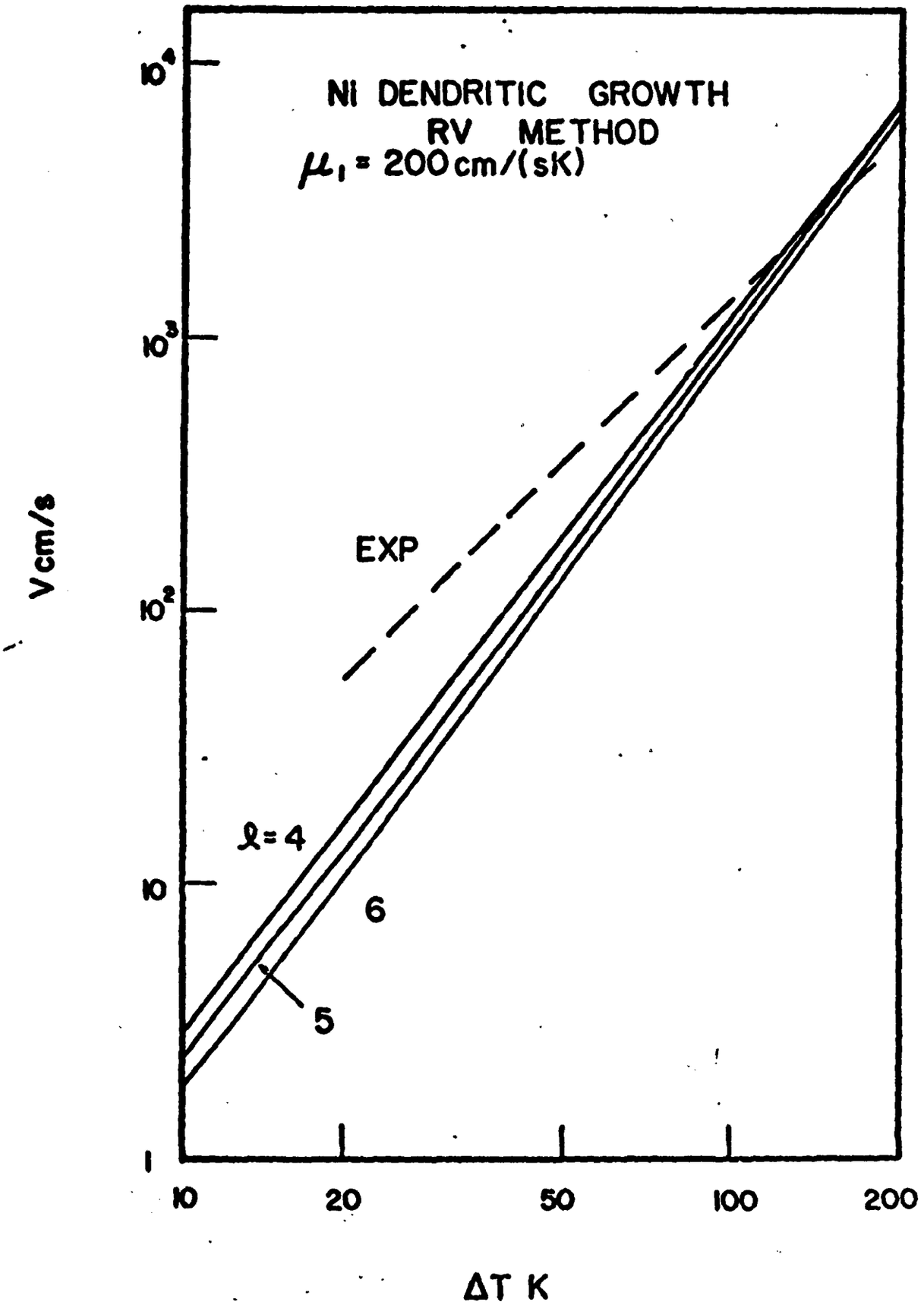
NI DENDRITIC GROWTH
RV METHOD
$\mu_1 = 200\,cm/(sK)$
EXP
$\ell = 4$
6
5
V cm/s
10^3
10^2
10
1
10
20
50
100
200
ΔT K